Formation of molecular ions by radiative association of cold trapped atoms and ions

Humberto da Silva Jr, Maurice Raoult, Mireille Aymar, Olivier Dulieu

Formation of molecular ions by radiative association of cold trapped atoms and ions

Humberto da Silva Jr.[1]

[1]Laboratoire Aimé Cotton, CNRS/Université Paris-Sud/ENS Cachan, Orsay Cedex, France

Maurice Raoult[1]

[1]Laboratoire Aimé Cotton, CNRS/Université Paris-Sud/ENS Cachan, Orsay Cedex, France

Mireille Aymar[1]

[1]Laboratoire Aimé Cotton, CNRS/Université Paris-Sud/ENS Cachan, Orsay Cedex, France

Olivier Dulieu[1]

[1]Laboratoire Aimé Cotton, CNRS/Université Paris-Sud/ENS Cachan, Orsay Cedex, France

E-mail: `olivier.dulieu@u-psud.fr`

Abstract. Radiative emission during cold collisions between trapped laser-cooled Rb atoms and alkaline-earth ions (Ca^+, Sr^+, Ba^+) and Yb^+ are studied theoretically, using accurate effective-core-potential based quantum chemistry calculations of potential energy curves and transition dipole moments of the related molecular ions. Radiative association of molecular ions is predicted to occur for all systems with a cross section two to ten times larger than the radiative charge transfer one. Partial and total rate constants are also calculated and compared to available experiments. Narrow shape resonances are expected, which could be detectable at low temperature with an experimental resolution at the limit of the present standards. Vibrational distributions are also calculated, showing that the final molecular ions are not created in their ground state level.

1. Introduction

One of the novel developments of ultracold matter research is exemplified by the experiments aiming at merging a cold atom trap and a trap of laser-cooled ions. Such setups could offer the opportunity to study collisional dynamics in the quantum s-wave scattering regime associated to the long-range interaction between the ion and the atom

varying as R^{-4} (where R is the ion-atom distance) [1, 2, 3, 4], just like it has been extensively studied for ultracold neutral atom-atom collisions (see for instance Ref. [5]). Also, cold molecular ions could be created, opening the way to a rich chemistry at temperatures of a few millikelvin, or less [6]. Following the pioneering experiment of Ref. [7] with cold Na trapped in a magnetooptical trap (MOT) and laser-cooled Ca^+ ions in a Paul trap (then followed by further developments [8]), other groups have carried out similar experiments with improved detection efficiency: Yb atoms with Yb^+ ions [9], Rb atoms with Ca^+ [10, 11] and Ba^+ [12] ions, and Ca atoms with Yb^+ ions [13] or Ba^+ ions [14]. Rubidium atoms can also be confined in a magnetic trap in (or close to) the Bose-Einstein condensation (BEC) regime thus ensuring with a density larger than in a MOT, and then interacting with a few Yb^+ ions [15, 16, 17, 18]. Similarly, an optical dipole trap of Rb atoms has been merged in a Paul trap containing a few Ba^+ atoms [19, 20] (or with the combination Li/Ca^+ [21]). When atomic ions like Rb^+ or Na^+ cannot be laser-cooled, they can be sympathetically cooled by another species in the Paul trap in the presence of trapped Rb atoms [22, 20] or Na atoms [23], or they can be created *in situ* inside the Paul trap by photoionization of trapped Rb atoms [24, 25, 26]. A comprehensive review of most of these experiments can be found in Ref. [27].

Elastic and inelastic collisions as well as elementary reactions like charge transfer between the trapped ions and the trapped atoms have been studied in these experiments. Due to the residual micromotion of the trapped ions, these studies have been limited to energies larger than a few millikelvin, well beyond the s-wave quantum regime. It has been recognized in several of these experiments (see for instance Ref. [10]) that the cooling and/or trapping light most often assist the reaction through the excitation of one of the colliding partners, inducing large rates described by the Langevin regime close to the unitarity limit.

Among all these experiments, it is striking that so far, the direct observation of molecular ions resulting from the association of a cold atom and a cold ion has been reported only in two cases, namely $RbCa^+$ [10, 11] and $RbBa^+$ [12]. These observations have been assigned to the formation of ions by radiative association (RA), *i.e.* Rb + $(Alke)^+ \rightarrow Rb(Alke)^+ + h\nu$ (where (Alke) = Ca, Ba), and $h\nu$ is the energy of the photon emitted during the collision in order to stabilize the molecular ion [10, 11, 12]. The RA process competes with radiative charge transfer (RCT) Rb + $(Alke)^+ \rightarrow Rb^+ +$ (Alke) $+h\nu$ when (Alke) = Ba, and is dominated by non-radiative charge transfer (NRCT) in the Rb/Ca^+ case [28]. The RA of $CaYb^+$ has been invoked – but molecular ions have not been directly detected – in Ref. [13] to explain the measured fast reaction rate, but not confirmed by a subsequent theoretical investigation [29].

In order to clarify the possible molecular ion formation processes and their efficiency in such merged ion and atom traps, we achieved in this paper a systematic analysis of the inelastic collisions of cold $Rb/(Alke)^+$ pairs in their ground state (with (Alke) = Ca, Sr, Ba and Yb), considering the two competitive channels of RA and RCT. After recalling the basics of the derivation of expressions for the cross section and the rates

(Section 2), we describe the electronic structure (potential energy curves, transition and permanent electric dipole moments) of the relevant molecular ions Rb(Alke)$^+$ using accurate quantum chemistry calculations based on the representation of the colliding partners with effective core potentials (ECP) including core polarization potentials (Section 3) which are compared to other determinations when available. We present our results for both RA and RCT cross sections and rates, emphasizing then on the presence of narrow shape resonances induced by the centrifugal barrier in the entrance channel, and on the vibrational distribution of the molecular ions, which are not expected to be created in their ground level (Section 4). We finally discuss some prospects about possible explanation for the absence of molecular ions in several of the experiments quoted above.

In the rest of the paper atomic units of energy (1 a.u. $= 2 \times R_\infty$ where R_∞ is the Rydberg constant), distance (1 a.u. $= a_0$ where a_0 is the Bohr radii), and dipole moment (1 a.u. = 2.541 580 59 D) will be used, except otherwise stated. The collision energies will usually be expressed in units of (milli-)Kelvin, $E_{coll} \equiv E_{coll}/k_b$, where k_b is the Boltzmann constant.

2. Theoretical approach for RA and RCT

The spontaneous emission of a photon during a collisional process is modeled by a well-established formalism. It is a special case of a well-known semiclassical matter-radiation interaction scheme of absorption and emission. A 1^{st}-order time-dependent perturbation approach expresses the atomic or molecular transition between an initial state $|i\rangle$, with energy E_i in the instant t_i and a final state $|f\rangle$, with energy E_f at $t > t_i$, induced by the perturbation of the electromagnetic field $H' = H'(t > t_i)$. Such a methodology has been successfully applied to the description of the radiative association [30, 31, 32, 33, 29] and of the radiative charge transfer in atom-ion collisions, for elementary systems such as Li(2s) + H$^+$ [34]. In the following we only recall the main steps, and a full description can be found in the given references and the references therein.

In the collisions between ground-state (Alke)$^+(ns)$ ions ($n = 4, 5, 6, 6$ for Ca, Sr, Ba, Yb, respectively) and Rb($5s$) atoms, the entrance channel is associated with a single adiabatic Born-Oppenheimer (ABO) potential energy curve (PEC) $V_i(R)$ of $^1\Sigma^+$ symmetry which actually corresponds to the first excited electronic state $A^1\Sigma^+$ of the (Alke)Rb$^+$ molecular ion (Fig. 1a). The spontaneous emission during the collision thus leads either to the dissociation continuum (for RCT) or to the bound rovibrational level manifold (for RA) of the PEC $V_f(R)$ of the (Alke)Rb$^+$ ground electronic state $X^1\Sigma^+$ correlating to the lowest (Alke)($ns^2\,^1S$) + Rb$^+$ asymptote. Note that below the entrance channel there is an additional asymptotic limit only in RbCa$^+$, namely Rb$^+$ + Ca($4s4p\,^3P$), to which the PEC lowest $^3\Pi$ state is correlated and which is coupled to the A state by spin-orbit interaction, thus inducing non-adiabatic transition, *i.e.* NRCT [28]. This feature is not treated in the present paper. Also, as illustrated for instance in our previous work on alkali-metal atom and Sr$^+$ compounds [35], the lowest $^3\Sigma^+$ PEC

is correlated to the entrance channel (Alke)$^+(ns)$ + Rb($5s$), but cannot give rise to spontaneous emission to the X state, as long as no second-order spin-orbit coupling is introduced. The hyperfine structure of the colliding partners – which has been found to be an important feature in Ref. [15] – is neglected, so that the entrance channel $A^1\Sigma^+$ is assumed to be populated with a statistical weight of $p = 1/4$.

Following our previous investigation [36] and similar ones (see for instance Refs. [37, 32], the total spontaneous emission cross section during the collision at energy E_{coll} is formulated as the sum of two contributions from the RCT and RA processes

$$\sigma^{RCT}(\epsilon_i) = p\frac{8\pi^2}{3c^3}\frac{1}{k_i^2}\sum_{J=0}^{\infty}\int_0^{\epsilon_f^{max}}[\left(\omega_{i,f}^3 J|\langle J-1,\epsilon_f|D(R)|\epsilon_i,J\rangle|^2\right) + \left(\omega_{i,f}^3(J+1)|\langle J+1,\epsilon_f|D(R)|\epsilon_i,J\rangle|^2\right)]d\epsilon_f \quad (1)$$

$$\sigma^{RA}(\epsilon_i) = p\frac{8\pi^2}{3c^3}\frac{1}{k_i^2}\sum_{J=0}^{\infty}\sum_{v=0}^{v_{max}}[\left(\omega_{iJ,v(J-1)}^3 J|\langle J-1,v|D(R)|\epsilon_i,J\rangle|^2\right) + \left(\omega_{iJ,v(J+1)}^3(J+1)|\langle J+1,v|D(R)|\epsilon_i,J\rangle|^2\right)] \quad (2)$$

All the quantities in these equations are expressed in atomic units. In Eq. (1) the integral is limited to the largest possible energy ϵ_f^{max} in the exit channel, while in Eq. (2) the summation is limited to the uppermost vibrational level v_{max} of the X state. The initial ket $|\epsilon_i, J\rangle$ with energy $\epsilon_i = E - V_i(R = \infty)$ and associated wavenumber $k_i = \sqrt{2\mu\epsilon_i}$ (μ is the reduced mass of the (Alke)Rb$^+$ system) represents a partial-wave component J of an energy-normalized continuum wavefunction of the two nuclei. As only $^1\Sigma^+$ states are involved, J is the total angular momentum in the entrance channel, and $J' = J \pm 1$ are the two possible allowed total angular momenta in the exit channel. In both equations above, the summation on J is actually limited for each collisional energy to the maximal value for which the induced rotational barrier in the entrance channel prevents the collision to occur. The transition electric dipole moment (TEDM) function $D(R)$ is represented in Figure 1b for each system.

For RCT the final state is represented by $|\epsilon_f, J \pm 1\rangle$ with energy $\epsilon_f = E - V_f(R = \infty) - \hbar\omega_{if}$, where ω_{if} is the energy of the emitted photon. Equation 1 contains the transition dipole moment between $|\epsilon_i, J\rangle$ and $|\epsilon_f, J'\rangle$

$$\langle J', \epsilon_f|D(R)|\epsilon_i, J\rangle = \int_0^{\infty} F_{J'}^f(\epsilon_f, R)D(R)F_J^i(\epsilon_i, R)\, dR \quad (3)$$

involving two energy-normalized continuum wave functions $F_J^i(\epsilon_i, R)$ and $F_{J'}^f(\epsilon_f, R)$. At large distances they behave like

$$F_\ell(\epsilon, R) \sim \sqrt{\frac{2\mu}{\pi k}}\sin(kR - \ell\frac{\pi}{2} + \delta_\ell) \quad (4)$$

For RA the final state $|v, J\rangle$ is a bound rovibrational level of the $X^1\Sigma^+$ ground electronic state of the (Alke)Rb$^+$ molecular ion. The corresponding transition dipole moment is

$$\langle J', v|D(R)|\epsilon_i, J\rangle = \int_0^{\infty} \chi_{vJ'}^f(R)D(R)F_J^i(\epsilon_i, R)\, dR \quad (5)$$

where χ_v is a radial rovibrational wave function of the molecule normalized to unity.

Our calculations cover an energy range in the entrance channel from 1 mK up to 80 mK, currently accessible in most experiments. This requires to consider J values in the range [15;40], [20;50], [20;50], and [20;55] for $RbCa^+$, $RbSr^+$, $RbCa^+$, and $RbYb^+$ respectively, in order to obtain converged cross sections. The integrations over the internuclear distance R are performed with the Milne phase-amplitude method [38, 39]. Such high J values and low initial temperature impose to propagate out the continuum wave function in the entrance channel up to large R values, namely 20000 a.u. This insures that the outward propagation is stopped well within the classically allowed region situated at long range beyond the centrifugal barrier. The upper limit $\epsilon_f^{max} = 1000$ cm^{-1} of the relative energy in the integral of Eq. (1) and the integration step $d\epsilon_f = 1$cm^{-1} are taken to insure the integral convergence.

Anticipating on the results of Section 4, Fig. 2a illustrates this well-known feature in the case of $RbSr^+$, where examples of radial wave functions are drawn for three collision energies: (i) at 0.08 cm^{-1}, above the centrifugal barrier; (ii) at 0.015 cm^{-1}, showing a major tunneling through the barrier, (iii) at 0.01 cm^{-1}, with no more tunneling. The last two cases correspond to the Wigner threshold law energy range, and the related partial cross sections reported in Fig. 2b present an energy dependence proportional to k^2 as expected for high partial wave value associated with a R^{-4} long-range interaction. The wave function of type (ii) above gives rise to sharp shape resonances with widths from a fraction of μK up to about 4 mK, requiring a very small energy step (2μK) to locate them. The first case depicts a regime similar to the Langevin one, with the same k^{-1} energy dependence of the cross-section at high energy in every partial wave, but with a magnitude smaller than the one predicted by the Langevin model (see Section 4). Note also the alternation of the occurrence of the shape resonances: if a shape resonance shows up for the partial wave ℓ, another also occurs for the $\ell + 2$ partial wave as demonstrated by B.Gao in the case of a R^{-4} long range interaction [40].

3. Electronic structure calculations for Rb(Alke)$^+$ molecular ions

The potential energy curves, permanent electric dipole moments (PEDMs) and transition electric dipole moments are computed following the same method described in details in Ref. [41, 35]. We briefly recall here the main steps of the calculations, carried out using the Configuration Interaction by Perturbation of a Multiconfiguration Wave Function Selected Iteratively (CIPSI) [42] package developed at "Universit*é* Toulouse III - Paul Sabatier" (France). The Rb + (Alke)$^+$ system (where Alke is a neutral alkaline-earth atom among Ca, Sr, Ba, and by extension, Yb) is modeled as a molecule where two valence electrons move in the field of the Rb^+ and $(Alke)^{2+}$ ions represented with ECPs including relativistic scalar effects. These ECPs are taken from Refs. [43, 44] for all species but Sr^{2+} and Ba^{2+} [45, 46] and Yb [47]. The ECPs are complemented with core polarization potentials (CPPs) depending on the orbital angular momentum ℓ of the valence electron of Rb and (Alke)$^+$ [48, 49], and parametrized with the Rb^+

and $(\mathrm{Alke})^{2+}$ static polarizabilities α and two sets of three cut-off radii ρ_s, ρ_p, and ρ_d. All these parameters (except for Yb^+) were used in our previous work on alkali dimers [41, 50] and on alkaline-earth hydride ions [51]. The value for the Yb^{2+} polarizability is $\alpha = 6.388$ a.u. [52], and the cut-off radii $\rho_s = 1.8869$ a.u., $\rho_p = 0.89235$ a.u., and $\rho_d = 2.051150$ a.u. have been adjusted to reproduce the experimental energies of the $f^{14}6s$, $4f^{14}6p$ and $4f^{14}5d$ states of the Yb^+ ion [53]. Only the remaining two valence electrons are used to calculate the Hartree-Fock and the excitation determinants, in an atom-centered Gaussian basis set, through the usual self-consistent field methodology. The basis set used for the Rb atom is from Refs.[41, 54] and from Ref. [51] for the $(\mathrm{Alke})^+$ ions (except for Yb^+). We used for Yb^+ a large uncontracted $(5s5p6d)$ Gaussian basis set with the series of exponents (0.785942, 0.370489, 0.068843, 0.031984, 0.015622), (0.685598, 0.338376, 0.073598, 0.034232, 0.015836) and (1.377363, 0.785942, 0.492827, 0.1680780, 0.058334, 0.02) for s, p, and d orbitals, respectively. It is worthwhile to note that to our knowledge this is the first time that the Yb^+ ion is represented in a so-called "'large core"' model, apart from Ref. [47]. A more detailed analysis of the $(\mathrm{Yb\text{-}Alk})^+$ compounds (where Alk is an alkali-metal atom among Li, Na, K, Rb, Cs) will be presented in a forthcoming study.

A full configuration interaction (FCI) is finally achieved to obtain the relevant PECs and TEDMs displayed in Fig. 1, limited to the X and A states and their transition. The origin of energies is taken at the $(\mathrm{Alke})^+(ns)$ + Rb$(5s)$ dissociation limit corresponding to the entrance channel relevant for the present study. By construction the dissociation energy matches the experimental one in the former case, while for the latter case it results from the CI calculation performed on the neutral (Alke) atom. These (Alke) ground state binding energies are reported in Ref. [51] for all atoms except Yb, where we obtained a value smaller by 115 cm^{-1} compared to the experimental one.

All PECs for the A state consistently behave in the same way at large distances (Fig. 1a), varying as $-C_4/(2R^4)$ determined by the Rb static polarizability $\alpha_{\mathrm{Rb}} \equiv 2C_4$. A rough fit with a single parameter of the long-range part of the PECs yields $2C_4 \approx 360 \pm 20$ a.u. depending on the species, while a more relevant determination using the approach above in the context of the finite field method yields $2C_4 = 318$a.u. [55] in good agreement with the various determinations of the Rb static polarizability [56]. The well-depth decreases with increasing mass along the series Ca, Sr, Ba. In agreement with other determinations [57, 58, 4], the $RbBa^+$ PEC exhibits a double well induced by an avoided crossing with an upper $^1\Sigma^+$ curve not displayed here. This feature is imprinted in the variation of the corresponding A-X TEDM (Fig. 1c). Surprisingly, the PEC of $RbCa^+$ and $RbYb^+$ are very similar, which could be related to the well-known f-shell contraction in the lanthanide atoms, yielding to the Yb the character of a much smaller atom than expected from its mass [59].

The PECs for the X state all look very similar along the series (Fig. 1b). As above, the long-range part of the PEC varies as R^{-4}, with a coefficient depending on the static polarizability of the (Alke) neutral species. Again, a simple fit of this long-range part with a single parameter gives $2C_4 \approx 140$ a.u., 220 a.u., 300 a.u., and 154

a.u., for $RbCa^+$, $RbSr^+$, $RbCa^+$, and $RbYb^+$ respectively, in reasonable agreement with the static polarizabilities of Ca, Sr, Ba, and Yb from our previous calculations [51] or from [56]. Note that to determine more rigorously these quantities within our quantum chemistry approach, a method like the finite-field approach should be used, as we have done for instance in the Sr case [35].

The main spectroscopic constants of these PECs are deduced from a parabolic fit of the bottom of the wells around their minimum, and are reported in Tables 1 and 2, allowing for comparison with the few other theoretical determinations available in the literature. The choice of isotopes is somewhat arbitrary, as it has no significant influence on the scattering calculations, as it will be discussed later.

There is only one other work reporting about the molecular structure of $RbCa^+$ [28, 60] for the study of NRCT. The authors used a so-called "'small core"' ECPs where electrons from the $4s$ and $4p$ shells in Rb, and from the $3s$ and $3p$ shells in Ca^+ are explicitly treated besides the valence electrons. As for the $^1\Sigma^+$ states, the authors only provided figures for the PECs from which we estimated equilibrium distances and potential well depths in good agreement with our results. This is a strong indication in favor of the ability of our approach employing large core ECPs to represent core-valence electronic correlation.

The $RbBa^+$ molecule already attracted several detailed non relativistic studies which are in quite good agreement among each other. We observe the same trend than for $RbCa^+$, *i.e.* for both X and A states we find slightly smaller equilibrium distances, and slightly deeper potential wells than in Refs. [57, 58, 4]. In Ref. [4] the authors investigated the role of the triple excitations in their approach, yielding a double-well potential for the A state with a barrier located below the dissociation limit at about the same position (estimated from their figure) than in our calculation. Again, this is a strong argument in favor of the present approach based on ECP and CPP to represent correctly core-valence correlation effects.

For $RbSr^+$, there is no other calculation available than [35], but given the favorable comparisons above, and as this ion is treated consistently with the same method than the three other species, the present results are probably of satisfactory quality.

As already quoted above, the case of $RbYb^+$ is peculiar, as the Yb^+ ion has never been treated with large ECP before. Tables 1 and 2 reveal a contrasted situation in comparison with the results of Refs. [61, 62, 63] obtained with similar approaches bases on small core ECPs. Our values for R_e and D_e of the X PEC are in good agreement with those of Ref. [63], while the potential well depth from Refs. [61, 62] is twice smaller than ours, with a minimum located at a significantly larger distance. This has been quoted by the authors of Ref. [62] but no explanation has been provided. On the other hand for the A state, the three previous papers have obtained results in good agreement among each other, while we find an equilibrium distance shorter by about 1a.u. and the well depth deeper by about 400 cm^{-1}. But the magnitude and the R variation of the TEDM of the X-A transition look very similar among all determinations, with a maximal value of about 3 a.u., suggesting that electronic wave functions behave in the

same way in all methods.

Table 1. Main spectroscopic constants for the $X^1\Sigma^+$ electronic state of [Rb-(Alke)]$^+$: the bond length, r_e (a. u.), the harmonic constant, ω_e (cm^{-1}), the potential well depths, D_e (cm^{-1}), the rotational constant, B_e (cm^{-1}). Other published values are also provided when available. Two sets of results were published in Ref. [58], (a) using a multireference configuration interaction (MRCI), and (b) using the coupled-cluster method.

$(X)^1\Sigma^+$	r_e	ω_e	B_e	D_e
$^{87}Rb^{40}Ca^+$				
this work	7.96	73.02	0.0346	3850.9
[28]	≈8.0	-	-	≈3730
$^{87}Rb^{87}Sr^+$				
this work	8.23	59.41	0.0205	4265.7
[35]	8.2	58	-	4285
$^{87}Rb^{137}Ba^+$				
this work	8.53	51.01	0.0155	5292.5
[58]^a	8.72	51.77	-	5055.0
[58]^b	8.75	52.79	-	5034.0
[4]	8.67	-	-	5136
$^{87}Rb^{173}Yb^+$				
this work	7.99	49.73	0.0162	3435.88
[63]	8.08	-	-	3496
[61]	9.03	33.77	0.0127	1776
[62]	9.0	-	-	1807.4

For completeness we report in Fig. 3 the PEDMs for both the A and X states of these molecular ions. They have been computed with respect to the origin of coordinates placed at the center-of-mass of the molecule, with the axis oriented from the Rb atom towards the $(Alke)^+$ ion. We note the total mass $M = M(Rb^+) + M(Alke)$ and the mass difference $\delta M = M(Rb^+) - M(Alke)$. At large distances, the PEDMs linearly diverge as $R/2(1 + \delta M/M)$ and $-R/2(-1 + \delta M/M)$ with for the A and X states respectively, as the charge is carried either by the (Alke) species or by Rb. The PEDM of the A state in $RbBa^+$ has an abrupt change of slope around 12a.u. due to the occurrence of the barrier between the two potential wells.

The data for PECs, TEDMs, and PEDMs are collected in the Supplemental Material attached to this paper.

4. Cross sections and rates for RA and RCT

The main objective of this study is to evaluate, through the comparison of four molecular ions treated consistently by the same approaches for both their electronic structure and

Table 2. Same as Table 1 for the $A^1\Sigma^+$ electronic states of [Rb-(Alke)]$^+$. In addition the transition energy T_e (cm^{-1}) between the bottom of the A and X potential wells is reported. For $RbBa^+$, values for the inner and outer wells are displayed on the same line. The position of the top of the barrier, and its energy below the dissociation limit, are also indicated.

$(A)^1\Sigma^+$	r_e	ω_e	B_e	D_e	T_e
$^{87}Rb^{40}Ca^+$					
this work	12.86	29.89	0.0133	1271.64	18171.2
[28]	≈13	-	-	≈1170	-
$^{87}Rb^{87}Sr^+$					
this work	13.8	21.04	0.0073	933.4	15752.3
[35]	13.8	21	-	960	-
$^{87}Rb^{137}Ba^+$					
this work (inner/outer)	8.97/14.81	40.49/15.94	0.0140/0.0051	964.81/679.27	12849.8/13135.3
this work (barrier)	11.61	-	-	65.3	-
[58]^a	9.03	-	-	-	-
[58]^b			-		
[4] (inner/outer)	9.02/15.19	-	-	911/576	12569/12904
$^{87}Rb^{173}Yb^+$					
this work	12.82	21.08	0.0063	1258.25	19138.2
[63]	13.8	-	-	836.0	-
[61]	14.362	16.807	0.00505	875.1	-
[62]	14.0	-	-	875.1	-

their dynamics, the efficiency of the formation of molecular ions, and the possibility to observe shape resonances with the current experimental resolution. Thus our results are presented such that a direct comparison can be easily made, the systems being ordered according to their increasing reduced mass. We performed about 40000 calculations per system in the collisional energy range between 100 μK to 80 mK, for all the total rotational quantum numbers between 0 and 80. The energy step was fixed to 2μK in order to properly locate all the shape resonances.

Figure 4 displays the total cross sections (RA + RCT) for all four systems, which present several similar features. As anticipated in section 2 they all present the same $\epsilon_i^{-1/2}$ dependence with the entrance channel energy ϵ_i which corresponds to the Langevin-type regime. However the magnitude of the cross sections is much smaller than the one

predicted by the original Langevin model [64]

$$\sigma_L = P\pi\epsilon_i^{-1/2}\sqrt{2C_4} \tag{6}$$

with a reaction probability P following the capture equal to 1. As the baseline of our calculated cross sections (*i.e.* ignoring shape resonances) varies as $\epsilon_i^{-1/2}$, we find a constant probability $P = 1.7 \times 10^{-5}$, 8.8×10^{-6}, 6.6×10^{-6}, and $P = 1.8 \times 10^{-5}$, for $RbCa^+$, $RbSr^+$, $RbBa^+$, and $RbYb^+$, respectively.

Numerous narrow shape resonances arising from the entrance channel can be observed in every system, with a density increasing with the reduced mass. The resonances have obviously an energy position which dramatically depends on the calculated potential. Apart from the resonances, the hierarchy of the cross sections reflected by their baselines simply reflects the increasing magnitude of the ω_{if}^3 factor in Eqs. (1) and (2) along the series $RbBa^+$, $RbCa^+$, $RbSr^+$, and $RbYb^+$, which can be roughly appreciated from the relative position of the X PECs in Fig. 1.

The RA process is predicted to dominate for all systems in comparison with RCT, by a factor $\approx$ 2.4 for $RbCa^+$, $\approx$ 3.8 for $RbSr^+$, $\approx$ 13.6 for $RbBa^+$, and $\approx$ 2.2 for $RbYb^+$. This is due to the favorable relative position of the X and A potential wells which are too shifted against each other in R, so that the classical inner turning point of the A potential is aligned with the one of quite deeply bound levels of the X potential (see dotted lines in Fig. 1). The very similar behavior between $RbCa^+$ and $RbYb^+$ reflects the strong similarities of the PECs and TEDMs functions. The RA process is favored in $RbBa^+$ due to the double well in the A potential curve, which enhances the spontaneous emission towards X bound levels around the top of the barrier where the TEDM is important. In all cases, the shape resonances in the RA and RCT cross sections are the same, as they are due to the centrifugal barrier in the entrance channel (see also Refs. [60, 63]. In the framework of the present model, the choice of the isotopologues for each ionic species will not yield significantly different cross sections in magnitude, as the reduced mass (which differ by less than one percent among a series of isotopologues of a given ion) is involved only through the kinetics described by the radial wave functions. Sayfutyarova *et al.* reached the same conclusion for isotopologues of $RbYb^+$. But of course, the energy positions of the shape resonances will vary with the chosen isotopologue.

In Fig. 6 are presented the vibrational distributions of the ground state vibrational levels v_X produced by RA for all species, in the $J = 1$ case and ϵ_i =1 mK as a representative example. The fraction of population of a given vibrational level v_X of the X state, is defined as the ratio of the matrix element in Eq. (2) for $J = 1'$ and $v = v_X$, divided by the sum over all vibrational levels of the X state, for $J' = 1$, of the matrix elements. As expected, these distributions are similar for the three ions $RbCa^+$, $RbSr^+$, and $RbYb^+$, due to their similar electronic structure. The peak in the distributions fulfills the Franck-Condon principle as it is located at a transition energy close to the energy difference between the inner classical turning point of the A potential (located in the 10-12 a.u. range) and the outer turning point of the X potential (see vertical

dotted lines in Fig. 1. In contrast, the double-well pattern in $RbBa^+$ is manifested by a distribution extended to much lower vibrational levels than for the other species, due to the inner turning point of the A potential located around 8a.u.. The vibrational distribution is double-peaked as well, the peak at low v_X (resp. high v_X) corresponding to the energy difference between the inner classical turning point of the A potential and the inner (resp. outer) turning point of the X potential. The peak at low v_X is small however, due to the small magnitude of the TEDM in the corresponding distance range (see Fig. 1c).

Nevertheless, the molecular ions are all predicted vibrationally hot, as well as rotationally hot given the number of partial waves involved in the present energy range, even around 1 mK where many partial waves are still involved. Due to their PEDM (Fig. 3) they can radiatively decay in principle down two lower vibrational levels. We computed the radiative lifetime of a given level v for decaying down to the level $v-1$ for all systems, and found that it always exceeds 10 s because of the slow R variation of the PEDM.

In an attempt to mimic the measured rate constant behavior as a function of the collision energy, the total cross sections (RA + RCT) above have been convoluted with a Gaussian energy distribution with a 2 mK half-width (Fig. 7). As expected from the $\epsilon_i^{-1/2}$ variation of the cross sections, the obtained rates are almost constant over the 1 mK-80 mK collision energy range. Such a width for the energy distribution has not yet been reported in the experimental works published up to now, but it should be soon under reach. Also the energy distribution of the ions in a Coulomb crystal where molecular ions are –if observed– sympathetically cooled by the laser-cooled ions, has not a Gaussian form (see Refs. [10, 11, 12]) and could be actually much larger than 2 mK. In Fig. 8 the total rate constant for $RbSr^+$ is convoluted with Gaussian distributions of half-width varying from 1 mK to 5 mK, showing that the detection of shape resonances would be possible only with an improved energy resolution compared to current experiments.

5. Discussion and prospects

In the experiments quoted in the introduction, the rate measurements are based on the observation of the decreasing of the number of trapped laser-cooled ions with time, due to all possible processes. In some cases, a careful analysis of the data allows for extracting a rate for a particular process. Before discussing the comparison with the published experimental results, it is first worthwhile to check the consistency among all theoretical studies focusing on the radiative processes (RA and RCT) occurring during the collision between two ground state particles.

The dashed lines in Fig. 7 indicates the average level of the calculated total radiative rates (RA + RCT), yielding 3.1×10^{-14} cm^3/s, 1.9×10^{-14} cm^3/s, 1.2×10^{-14} cm^3/s, and 3.1×10^{-14} cm^3/s, for $RbCa^+$, $RbSr^+$, $RbBa^+$, and $RbYb^+$, respectively. The remarkably close values of these rates along the species is well understood from the similarities of

their electronic structure invoked earlier, while their differences play only a minor role. This is exemplified by the results from Refs. [63, 62] of 2.9×10^{-14} cm^3/s for the RA + RCT rate in RbYb$^+$, where the large difference of the A potential well compared to the present one only slightly influences the final rate, as the main contribution is controlled by the inner classical turning point of the PEC. The magnitude of the present rates is also consistent with the smaller theoretical rate of 1.5×10^{-15} cm^3/s computed for the same processes in Ca-Yb$^+$ mixture [29], as the energy difference δR^t_{X-A} between the inner classical turning point of the $A^2\Sigma^+$ potential curve in the entrance channel, and the outer classical turning point of the $X^2\Sigma^+$ potential curve in the exit channel is smaller (about 9000 cm^{-1}) than in the present series of species. Similarly, Makarov *et al.* modeled the same processes in Na-Ca$^+$, and obtained a total rate of 2.3×10^{-16} cm^3/s which reflects the quite small difference $\delta R^t_{X-A} \approx 10700$ cm^{-1} combined with a significantly smaller TEDM of about 0.6 a.u. compared to the present cases.

As visible from Fig. 1a the case of RbCa$^+$ is peculiar, due to the presence of the $b^3\Pi$ state dissociating to the Rb$^+$+Ca($4s4p\,^3P$) limit which is energetically open to the entrance channel. Tacconi *et al.* modeled the non-adiabatic coupling related to the spin-orbit interaction between the $b^3\Pi$ state and the $A^1\Sigma^+$ state, thus inducing non-radiative charge transfer (NRCT) which is predicted to dominate the dynamics of the charge exchange process. We note that this process cannot lead to subsequent radiative formation of molecular ions due to spin selection rule. In a further work [60], the NRCT cross sections are found to approximately vary as expected by the Langevin model as $\epsilon_i^{-1/2}$, and to exhibit shape resonances of the same kind than those expected in the RA and RCT cross sections, due to the centrifugal barrier in the entrance channel. Over the present energy range, the NRCT cross section, is evaluated to be about 200 times larger than the total radiative cross section [10]. Around 2 K the NRCT rate is found of the same order of magnitude (3.5×10^{-12} cm^3/s) than the experimental rate, conservatively estimated to 2 to 3×10^{-12} cm^3/s [10, 11]. The possibility for NRCT has been also invoked in the Ca-Yb$^+$ system, with a rate evaluated to a few 10^{-14} cm^3/s [13].

As for the Rb-Yb$^+$ system, the experimental rates measured in Ref. [15] are $3\pm1\times10^{-14}$ cm^3/s and $4.5\pm1.5\times10^{-14}$ cm^3/s, corresponding to the ^{172}Yb$^+$ and the ^{174}Yb$^+$ isotope, respectively, and when Rb is prepared in the ($F=2, M_F=2$) hyperfine level (F being the total angular momentum including nuclear spin and M_F its projection on the magnetic field axis used for the preparation). While being in remarkable agreement with the present total radiative rate and those of Refs. [63, 62], the isotopic effect is much larger than the one predicted in the models. Actually the same group later discovered a huge effect of the initial preparation of the Rb atoms in a given hyperfine level, with a rate 35 times larger than the above one when Rb is in the ($F=1, M_F=1$) hyperfine level [18].

The situation for the Rb-Ba$^+$ system is somewhat intermediate in comparison with the two previous cases above. Indeed, there is no possibility for NRCT, and only an upper bound of 5×10^{-13} cm^3/s is given for the experimental rate in Ref. [12], compatible with the present calculation but suggesting that it is at most 40 times larger than the

calculated one. In another experiment with Rb atoms prepared in the $(F = 1, M_F = -1)$ state in an almost Bose-condensed sample, Schmid *et al.* [19] estimated an inelastic cross section presumably due to radiative processes between ground state particles in the range of 10^{-15} cm^2 to 10^{-14} cm^2 at about 30 mK, corresponding to rate 3 to 30 times larger than the calculated one.

To be complete with such comparisons with experimental results, it is worthwhile to mention the exceptional case of Ca-Yb$^+$ – not interpreted yet – where a considerable rate for inelastic collision between ground state particles of $\approx 2 \times 10^{-10}$ cm^3/s, *i.e.* of the same order of magnitude than quasi-resonant charge transfer reaction between an atom and an ion of the same species but different isotopes (Grier *et al.* [9] measured a rate of $\approx 6 \times 10^{-10}$ cm^3/s in Yb-Yb$^+$; see also Refs. [1, 26]).

Last but not least, beside this quite contrasted situation for the comparison between experimental rate for inelastic collisions and calculated rates for radiative processes, there is another puzzling and not yet understood feature in this kind of experiments: while the theoretical models all consistently predict that RA should dominate RCT, molecular ions are directly observed by mass spectrometry only in the experiments of Hall *et al.* on Rb-Ca$^+$ [10, 11] and Rb-Ba$^+$. An indirect detection of CaYb$^+$ has been also reported in Ref. [13]. This statement strongly suggests that the dynamic in such merged cold atom-cold ion traps is much more complicated than anticipated. Several elements may have a significant impact on the interpretation of the experimental results:

- The laser light used for cooling and trapping atoms and ions is recognized to have a strong influence on the measured rates, as inelastic processes with excited species may be very large (see for instance Refs. [10, 11, 12, 14]. Furthermore, such –quite intense– light could prevent the produced molecular ions to be detected before being photodissociated. On the theoretical side, such light-assisted processes may be tedious to describe accurately, as much more collision channels are open due to the presence of numerous excited electronic states (see for instance Ref. [10]) which this rely on the quality of quantum chemistry calculations.
- The quoted experiment are achieved with various conditions of atomic densities: Rb atoms are either trapped in MOT with a quite low density of a few 10^9atoms/cm^3, or in almost Bose-condensed gases with density up to 10^{11}atoms/cm^3. Therefore collisions between surrounding Rb atoms and the formed molecular ions could well occur, and they are strongly exoergic for all systems studied here (see Table 3), assuming that there is no activation potential barrier in the triatomic collisional complex which would prevent the reaction to occur. One product would be Rb_2^+ ions which are indeed observed in the Rb-Ca$^+$ experiment of Refs. [10, 11], and presumably present in the Rb-Ba$^+$ experiment of Ref. [12]. Note that charge exchange reactions between a Rb(Alke)$^+$ ion and a Rb atom is energetically forbidden due to the weak binding energy of the related Rb(Alke) neutral molecule.
- At high atomic density, three-body collisions could well occur, as it has been recently probed [22, 65]. Such processes may participate to the formation of molecular ions,

as well as to their destruction if they are radiatively created. Experiments of Ref. [19] on Rb-Ba^+ and of Ref. [15] on Rb-Yb^+ both use an almost Bose-condensed atomic sample and have not observed yet any molecular ions.

To summarize, the present work focused on the cold inelastic collisions inducing radiative decay between ground state Rb atoms and a series of ground state ionic species (Ca^+, Sr^+, Ba^+, Yb^+). The consistent treatment of these series of pairs with the same quantum chemistry approach and the same dynamical model allows for general conclusions about the magnitude of the rate constants, and the efficiency of the formation of cold molecular ions. Dynamical results for $RbSr^+$ are published here for the first time, as well as the modeling of a heavy diatomic compound containing Yb with a large core ECP. These results could stimulate future joint experimental and theoretical investigations. For instance, the detection of a couple of shape resonances in one of these systems would put strong constraints on its electronic structure. Photodissociation experiments of the produced molecular ions such like those performed on MgH^+ [66] could also provide more insight on their spectroscopy, and on their vibrational distribution (see for instance Ref. [67]).

The exploration of a family of such systems like in the present work where a Rb atom interacts with an ion of a given class allows for varying – discontinuously – a characteristic parameter of the system, its reduced mass, revealing then the changes in the dynamics while the nature of the interactions are similar over the entire series. The same study is already achievable on the series of (Alk)-Sr^+ (with (Alk) = Li, Na, K, Rb, Cs) species that we previously studied [35]. Based on the arguments developed in the present work, we can already draw some conclusions for this family:

- the $LiSr^+$ will not be favorable for the formation of deeply-bound molecular ion. Indeed, despite a noticeable TEDM of about 2a.u., the A PEC of the entrance channel – which is almost repulsive – has an inner turning point which coincides in position with the outer turning point of the uppermost vibrational levels of the X PEC. Moreover, the energy difference δR^t_{X-A} is quite small, lower than 3000 cm^{-1}.
- the $RbSr^+$ has been explicitly treated here, and the $NaSr^+$ and KSr^+ species smoothly progress toward the $RbSr^+$ with increasing δR^t_{X-A} concerning deeper vibrational levels
- the $CsSr^+$ case is specific: due to the large spin-orbit in $Sr(5s5p\,^3P)$, the entrance channel $Cs(6s)$ + $Sr^+(5s)$ is located at an energy of about 20 cm^{-1} and 200 cm^{-1} above the Cs^+ + $Sr(5s5p\,^3P_1)$ and the Cs^+ + $Sr(5s5p\,^3P_0)$ dissociation limits, respectively. Therefore, just like in the Rb-Ca^+ combination, NRCT should dominate the dynamics of this system.

In any case, a central goal remains to progress towards lower temperature in order to approach the quantum s-wave collisional regime, which will be of crucial importance for the understanding and the control of such collisions which clearly departs from the semiclassical Langevin model, and for improving theoretical models.

Table 3. Energies (in cm^{-1}) of the quoted atom-molecule complexes calculated as the sum of the binding energy of the atom and the potential well depth of the molecular ions, with respect to an origin of energy taken when all three atomic fragments (one Rb atom, one Rb^+ ion, one (Alke) atom) are at infinity. Note that the energy of the combination with a Rb^+ ion and a neutral Rb(Alke) molecule lies much higher in energy due to the weak binding energy D_e of the Rb(Alke) molecule: for instance, $D_e(RbSr) = 1073cm^{-1}$ [68, 69], $D_e(RbYb) = 656cm^{-1}$ [70].

Origin	System	Energy	System	Energy
$Rb+Rb^+ + Ca$	$Rb + RbCa^+$	-36850	$Ca + Rb_2^+$	-55412
$Rb+Rb^+ + Sr$	$Rb + RbSr^+$	-37976	$Sr + Rb_2^+$	-51858
$Rb+Rb^+ + Ba$	$Rb + RbBa^+$	-38984	$Ba + Rb_2^+$	-47959
$Rb+Rb^+ + Yb$	$Rb + RbYb^+$	-37221	$Yb + Rb_2^+$	-56369

Acknowledgments

This research is supported by the Marie-Curie Initial Training Network "'COMIQ: Cold Molecular Ions at the Quantum limit"' of the European Commission under the Grant Agreement 607491. Stimulating discussions with Robin Côté, Johannes Hecker Denschlag, Eric Hudson, and Stefan Willitsch are gratefully acknowledged. The scattering calculations have been achieved thanks to the computing facility cluster GMPCS of the LUMAT federation (FR LUMAT 2764) (http://www.gmpcs.lumat.u-psud.fr/) and to the high-performance computing center IDRIS of CNRS (http://www.idris.fr/).

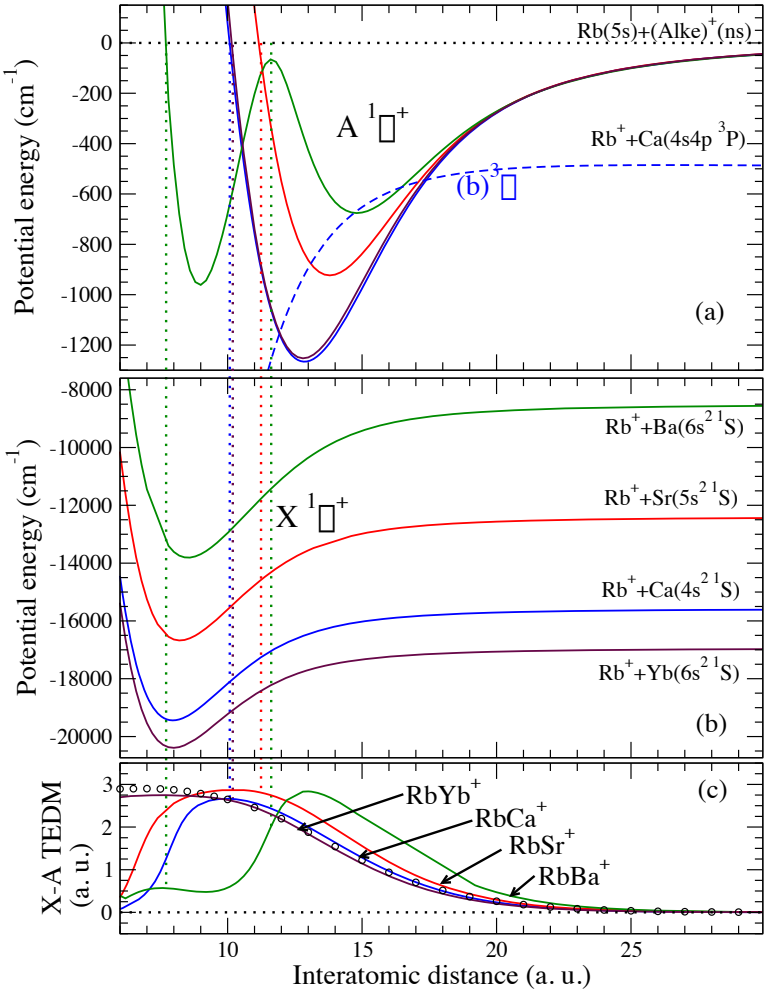

Figure 1. Potential energy curves of (a) the $A^1\Sigma^+$ state, and (b) of the $X^1\Sigma^+$ state, for the [Rb-(Alke)]$^+$ molecules, with (Alke) = Ca, Sr, Ba, and Yb. The origin of energies is taken at the dissociation of the $A^1\Sigma^+$ PEC for all systems. The lowest $^3\Pi$ PEC of Rb-Ca$^+$ is also displayed for completeness. (c) Transition electric dipole moments between the X and A states. Open circles: Ref. [62]. The vertical dotted lines tag the inner turning points of the incoming continuum wave function – in the entrance channel – with the respective points in the exit channel and the transition dipole moment magnitude at that position.

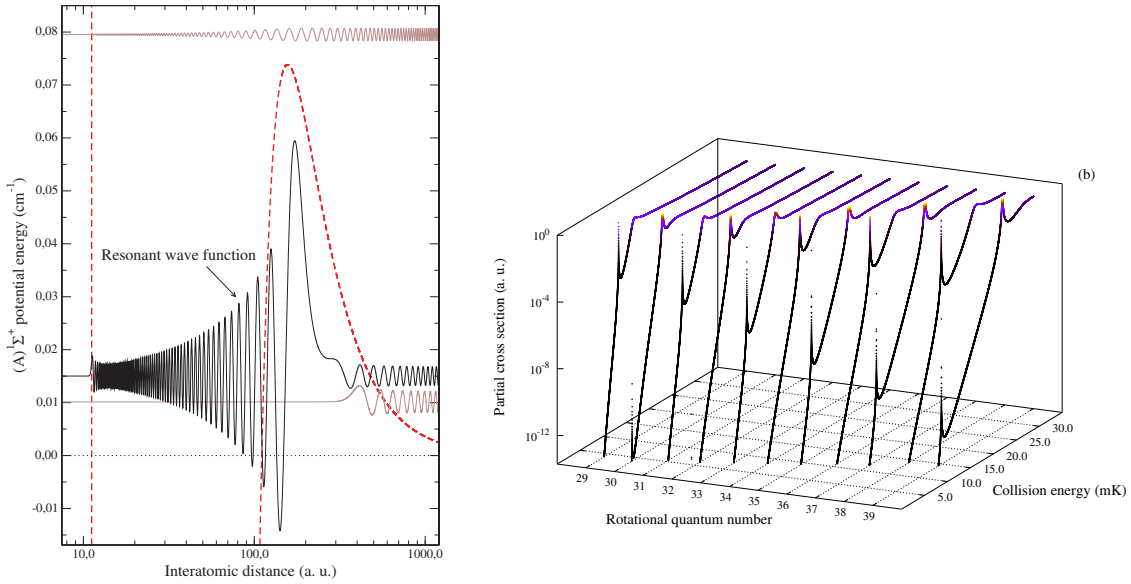

Figure 2. (a) Centrifugal barrier for $J = 35$ in the $A^1\Sigma^+$ potential energy curve of $RbSr^+$ (dashed line), with radial wave functions vertically placed at the appropriate collision energies, namely 0.08, 0.015, and 0.1 cm^{-1} to illustrate the various tunneling regimes. (b) Partial cross sections as a function of the collision energy (in mK) at 11 given values of rotational quantum numbers ($J' = 29$ to 39). Shape resonances gradually evolve with increasing J.

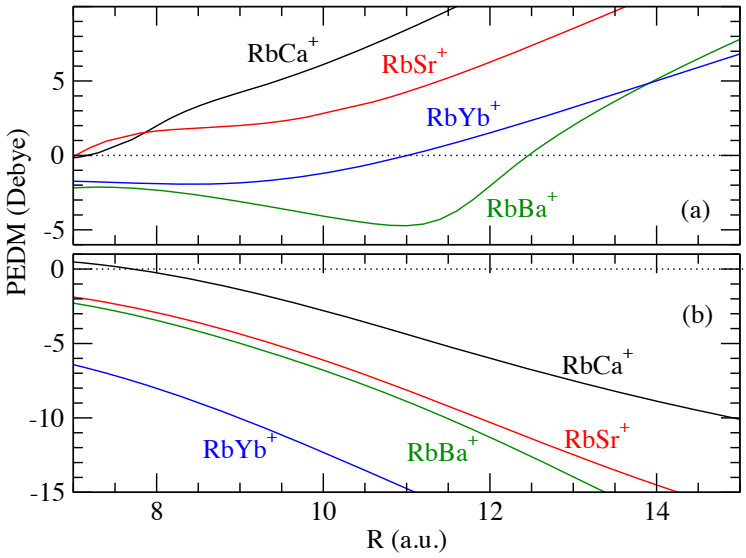

Figure 3. Permanent electric dipole moments of (a) the $A^1\Sigma^+$ state, and (b) of the $X^1\Sigma^+$ state, for the [Rb-(Alke)]$^+$ molecules, with (Alke) = Ca, Sr, Ba, and Yb.

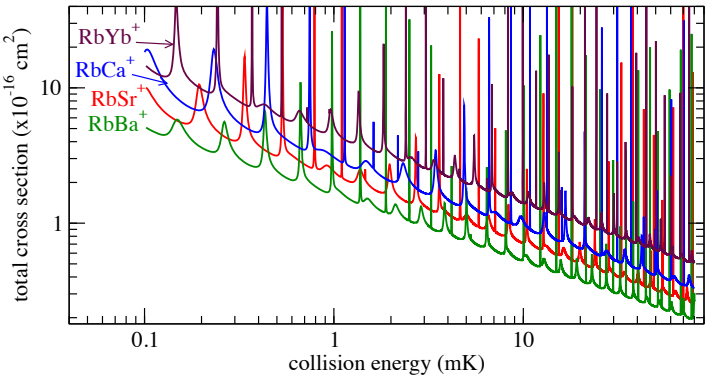

Figure 4. Calculated total cross sections (RA + RCT) (see Eqs. (1) and (2)) as functions of the collision energy (with both axes scaling logarithmically).

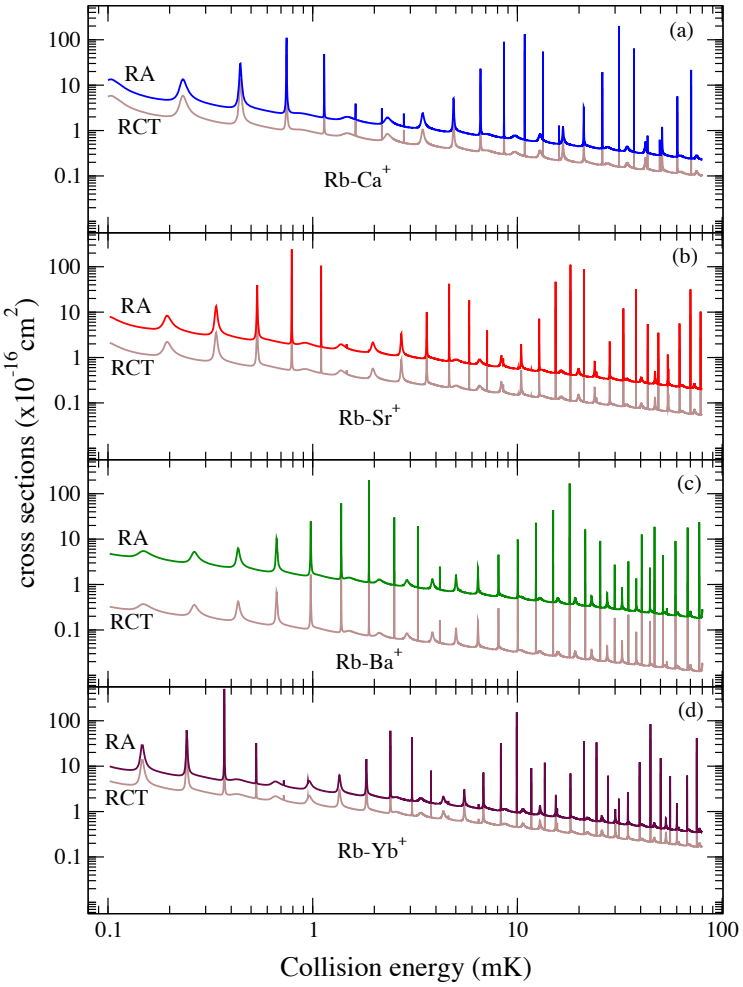

Figure 5. Calculated total cross sections as functions of the collision energy (with both axes scaling logarithmically), for radiative association (RA) and radiative charge transfer (RCT) (see Eqs. (1) and (2)).

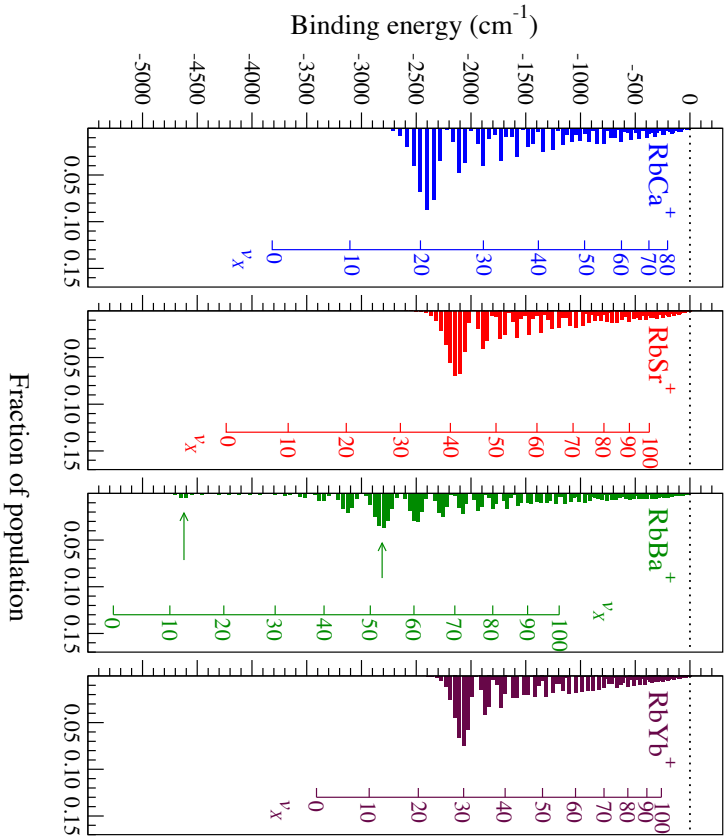

Figure 6. Calculated vibrational distributions of the ground state molecular ions produced by radiative association, as a function of the binding energies and the corresponding vibrational quantum numbers, v_X, for the rotational quantum number $J = 1$, at ϵ_i =1 mK. For comparison purpose, the energy scale is common for all species, and thus vibrational index are shifted from one species to the other.

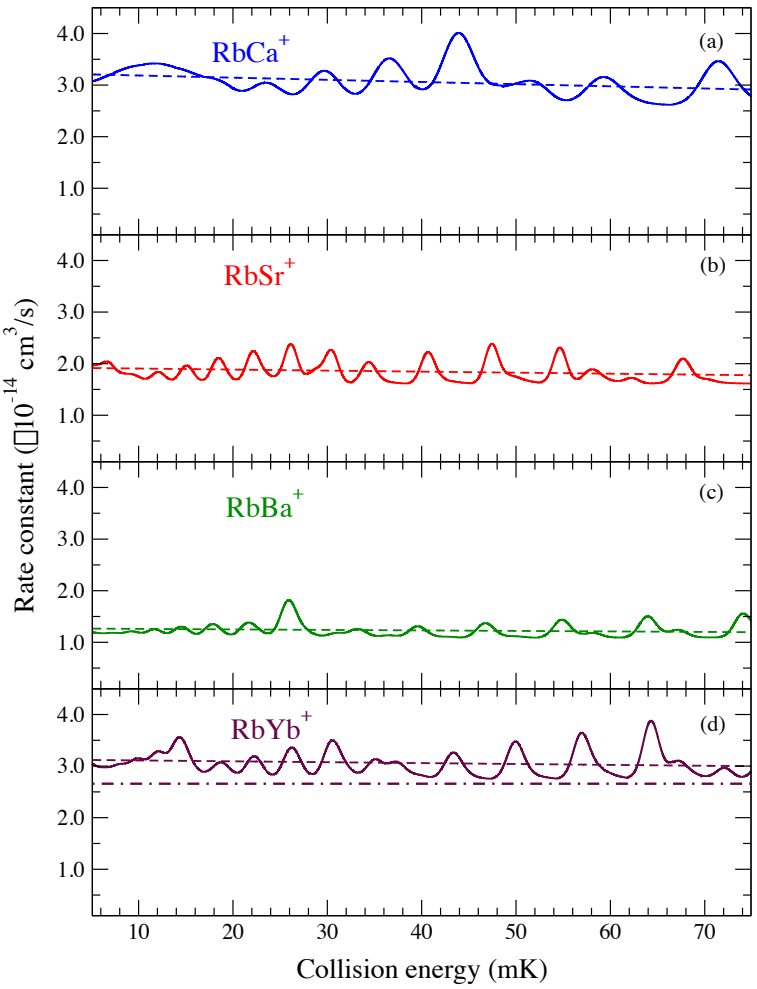

Figure 7. Calculated total (RA + RCT) rate constants convoluted from the cross sections of Fig. 4 with a Gaussian energy distribution of 2 mK half-width. The average level of these rates appears as the dashed lines. For $RbYb^+$, the calculated rate obtained in Ref. [63, 62] is indicated with a dot-dashed line.

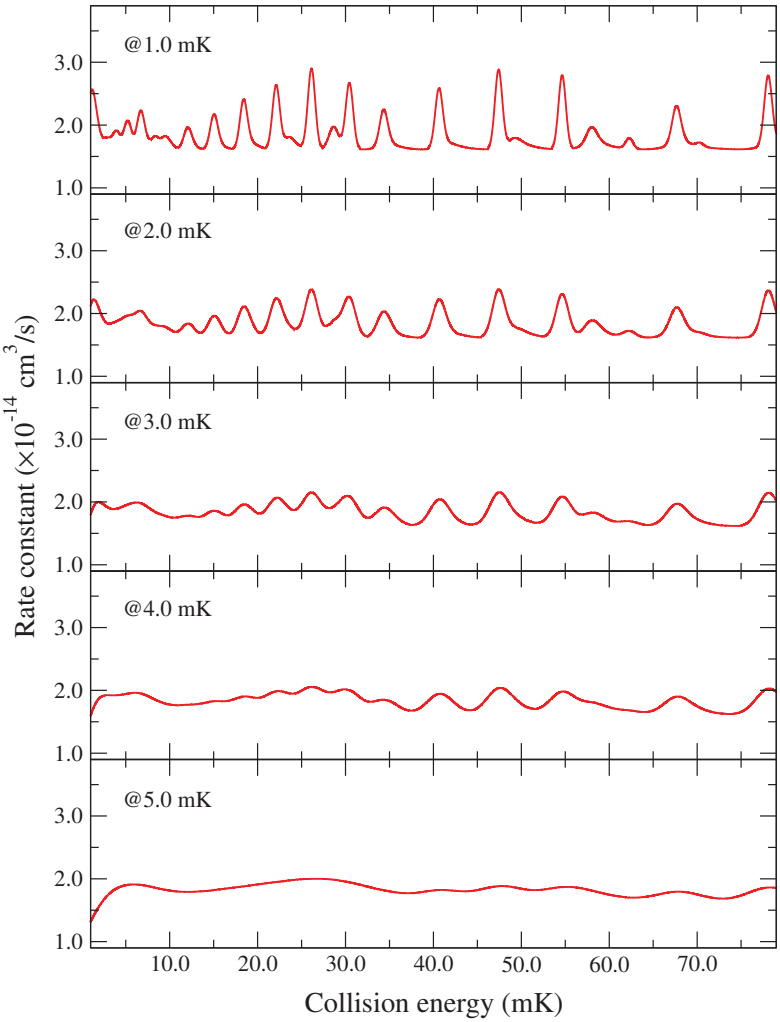

Figure 8. Calculated total rate constants for $RbSr^+$ convoluted with a Gaussian distribution half-width 1 mK to 5 mK.

[1] Côté R and Dalgarno A 2000 *Phys. Rev. A* **62** 012709
[2] Idziaszek Z, Calarco T, Julienne P S and Simoni A 2009 *Phys. Rev. A* **79** 010702
[3] Gao B 2011 *Phys. Rev. A* **83** 062712
[4] Krych M, Skomorowski W, Pawłowski F, Moszynski R and Idziaszek Z 2011 *Phys. Rev. A* **83** 032723
[5] Quéméner G and Julienne P S 2012 *Chem. Rev.* **112** 4949
[6] Willitsch S, Bell M T, Gingell A D, Procter S R and Softley T P 2008 *Phys. Rev. Lett.* **100** 043203
[7] Makarov O P, Côté R, Michels H and Smith W W 2003 *Phys. Rev. A* **67** 042705
[8] Smith W W, Goodman D S, Sivarajah I, Wells J E, Banerjee S, Côté R, Michels H H, Jr J A M and Narducci F A 2014 *Appl. Phys. B* **114** 75
[9] Grier A T, Cetina M, Oručević F and Vuletić V 2009 *Phys. Rev. Lett.* **102** 223201
[10] Hall F H J, Aymar M, Bouloufa N, Dulieu O and Willitsch S 2011 *Phys. Rev. Lett.* **107** 243202
[11] Hall F H, Eberle P, Hegi G, Raoult M, Aymar M, Dulieu O and Willitsch S 2013 *Molec. Phys.* **111** 2020
[12] Hall F H, Aymar M, Raoult M, Dulieu O and Willitsch S 2013 *Molec. Phys.* **111** 1683
[13] Rellergert W, Sullivan S, Kotochigova S, Petrov A, Chen K, Schowalter S and Hudson E 2011 *Phys. Rev. Lett.* **107** 243201
[14] Sullivan S, Rellergert W, Kotochigova S and Hudson E 2012 *Phys. Rev. Lett.* **109** 223002
[15] Zipkes C, Palzer S, Ratschbacher L, Sias C and Köhl M 2010 *Nature* **464** 308
[16] Zipkes C, Palzer S, Ratschbacher L, Sias C and Köhl M 2010 *Phys. Rev. Lett.* **105** 133201
[17] Zipkes C, Ratschbacher L, Palzer S, Sias C and Köhl M 2011 *J. Phys. Conf. Series* **264** 012019
[18] Ratschbacher L, Zipkes C, Sias C and Köhl M 2012 *Nature Phys.* **8** 649
[19] Schmid S, Härter A and Denschlag J H 2010 *Phys. Rev. Lett.* **105** 133202
[20] Schmid S, Härter A, Frisch A, Hoinka S and Denschlag J H 2012 *Rev. Sci. Instrum.* **83** 053108
[21] Haze S, Hata S, Fujinaga M and Mukaiyama T 2013 *Phys. Rev. A* **87** 052715
[22] Härter A, Krükow A, Brunner A, Schnitzler W, Schmid S and Denschlag J H 2012 *Phys. Rev. Lett.* **109** 123201
[23] Sivarajah I, Goodman D S, Wells J E, Narducci F A and Smith W W 2012 *Phys. Rev. A* **86** 063419
[24] Ravi K, Lee S, Sharma A, Werth G and Rangwala S 2012 *Appl. Phys. B* **107** 971–981
[25] Ravi K, Lee S, Sharma A, Werth G and Rangwala S 2012 *Nature Comm.* **3** doi:10.1038/ncomms2131
[26] Lee S, Ravi K and Rangwala S 2013 *Phys. Rev. A* **87** 052701
[27] Härter A and Hecker Denschlag J 2014 *Contemp. Phys.* **55** 33
[28] Tacconi M, Gianturco F A and Belyaev A K 2011 *Phys. Chem. Chem. Phys.* **13** 19156
[29] Zygelman B, Zelimir L and Hudson E R 2014 *J. Phys. B: At., Molec. Opt. Phys.* **47** 015301
[30] Zygelman B and Dalgarno A 1990 *Astrophys. J.* **365** 239
[31] Gianturco F A and Gori Giorgi P 1996 *Phys. Rev. A* **54** 4073
[32] Gianturco F A and Gori Giorgi P 1997 *Astrophys. J.* **479** 560
[33] Zygelman B, Stancil P C and Dalgarno A 1998 *Astrophys. J.* **508** 151
[34] Stancil P C and Zygelman B 1996 *Astrophys. J.* **472** 102
[35] Aymar M, Guérout R and Dulieu O 2011 *J. Chem. Phys.* **135** 064305
[36] Ayouz M, Lopes R, Raoult M, Dulieu O and Kokoouline V 2011 *Phys. Rev. A* **83** 052712
[37] Zygelman B and Dalgarno A 1988 *Phys. Rev. A* **38** 1877
[38] Milne W E 1930 *Phys. Rev.* **35** 863
[39] Korsch H J and Laurent H 1977 *J. Phys. B* **14** 4213
[40] Gao B 2013 *Phys. Rev. A* **88** 022701
[41] Aymar M and Dulieu O 2005 *J. Chem. Phys.* **122** 204302
[42] Huron B, Malrieu J P and Rancurel P 1973 *J. Chem. Phys.* **58** 5745
[43] Durand P and Barthelat J 1974 *Chem. Phys. Lett.* **27** 191
[44] Durand P and Barthelat J 1975 *Theor. chim. Acta* **38** 283
[45] Fuentealba P, von Szentpaly L, Preuss H and Stoll H 1985 *J. Phys. B: At. and Mol. Phys.* **18** 1287

[46] Fuentealba P and Reyes O 1987 *Molec. Phys.* **62** 1291
[47] Wang H, Gould P L and Stwalley W 1998 *Phys. Rev. Lett.* **80** 476
[48] Müller W, Flesch J and Meyer W 1984 *J. Chem. Phys.* **80** 3297
[49] Foucrault M, Millié P and Daudey J 1992 *J. Chem. Phys.* **96** 1257
[50] Aymar M and Dulieu O 2006 *J. Chem. Phys.* **125** 047101
[51] Aymar M and Dulieu O 2012 *J. Phys. B* **45** 215103
[52] Dzuba V A and Derevianko A 2010 *J. Phys. B At. Mol. Opt. Phys.* **43** 074011
[53] Ralchenko Y, Kramida A, J Reader J and Team N A 2014 Nist atomic spectra database (version 5.5) [online] (Gaithersburg, MD.: National Institute of Standards and Technology)
[54] Aymar M, Dulieu O and Spiegelman F 2006 *J. Phys. B: At. Mol. Opt. Phys.* **39** S905
[55] Deiglmayr J, Aymar M, Wester R, Weidemüller M and Dulieu O 2008 *J. Chem. Phys.* **129** 064309
[56] Derevianko A, Porsev S G and Babb J F 2010 *At. Data Nucl. Data Tables* **96** 323
[57] Knecht S, Jensen H J A and Fleig T 2008 *J. Chem. Phys.* **128** 014108
[58] Knecht S, Srensen L K, Jensen H J A, Fleig3 T and Marian C M 2010 *J. Phys. B* **43** 055101
[59] Cowan R 1981 *The theory of atomic structure and spectra* vol 3 (University of California Press)
[60] Belyaev A K, Yakovleva S A, Tacconi M and Gianturco F A 2012 *Phys. Rev. A* **85** 042716
[61] Lamb H, McCann J, McLaughlin B, Goold J, Wells N and Lane I 2012 *Phys. Rev. A* **86** 022716
[62] McLaughlin B M, Lamb H D L, Lane I C and McCann J F 2014 *Journal of Physics B: Atomic, Molecular and Optical Physics* **47** 145201
[63] Sayfutyarova E, Buchachenko A, Yakovleva S and Belyaev A 2013 *Phys. Rev. A* **87** 052717
[64] Langevin P 1905 *Ann. Chim. Phys.* **5** 245
[65] Härter A, Krükow A, Deiß M, Drews B, Tiemann E and Denschlag J H 2013 *Nature Phys.* **9** 512
[66] Bertelsen A, Vogelius I S, Jørgensen S, Kosloff R and Drewsen M 2004 *Eur. Phys. J. D* **31** 403
[67] Blangé J J, Zijlstra J M, Amelink A, Urbain X, Rudolph H, der Straten P V, Beijerinck H C W and MHeideman H G 1997 *Phys. Rev. Lett.* **78** 3089
[68] Guérout R, Aymar M and Dulieu O 2010 *Phys. Rev. A* **82** 042508
[69] Żuchowski P S, Guérout R and Dulieu O 2014 *Phys. Rev. A* **90** 012507
[70] Brue D and Hutson J 2013 *Phys. Rev. A* **87** 052709